

Elephant's Trunk Robot: An Extremely Versatile Under-actuated Continuum Robot Driven by a Single Motor

Yuwang Liu

State Key Laboratory of Robotics,
Shenyang Institute of Automation,
Chinese Academy of Sciences
114 Nanta Street, Shenyang
110016, P. R. China
liuyuwang@sia.cn

Zhuang Ge

School of Mechanical
Engineering and Automation,
Northeastern University
3 Wenhua Street, Shenyang
110819, P. R. China
gezhuang@sia.cn

Shangkui Yang

School of Mechanical
Engineering and Automation,
Northeastern University
3 Wenhua Street, Shenyang
110819, P. R. China
yangshangkui@sia.cn

Ian D. Walker¹

Department of Electrical and Computer
Engineering,
Clemson University
Clemson, SC 29634 USA
iwalker@clemson.edu

Zhaojie Ju

School of Computing,
University of Portsmouth
Buckingham Building, Lion Terrace,
Portsmouth PO1 3HE, UK
zhaojie.ju@port.ac.uk

ABSTRACT

Continuous-bodied “trunk and tentacle” robots have increased self-adaptability and obstacle avoidance capabilities, compared with traditional, discrete-jointed, robots with large rigid links. In particular, continuous-bodied robots have obvious advantages in grasping objects across a wide range of external dimensions. Not only can they grasp objects using end effectors like traditional robots, but their bodies can also be regarded as a gripping device, and large objects with respect to the robot’s scale can be captured by the entire structure of the robots themselves. Existing trunk-like robots have distributed multi-drive actuation, and are often manufactured using soft materials, which leads to a complex actuator system that also limits their potential applications in dangerous and extreme environments. This paper introduces a new type of elephant's trunk robot with very few driving constraints. The robot consists of a series of novel under-actuated linkage units. With a single motor drive, the robot can achieve stable grasping of objects of different shapes and sizes. The proposed robot simplifies the requirements of the sensing and control systems during the operation process, and has the advantage of accomplishing the capture task without determining the exact shape and position of the target object. It is especially suitable for operations such as non-cooperative target capture in extremely dangerous environments, including those in outer space. Based on theoretical analysis and model design, a trunk robot prototype was developed, and a comprehensive experimental study of the bending/extension and grasping operation functions was conducted to verify the validity of the proposed robot design.

¹ Ian D. Walker, Department of Electrical and Computer Engineering, Clemson University, Clemson, USA. E-mail: iwalker@clemson.edu.

1 INTRODUCTION

Compared to conventional robots with a small number of large rigid links connected at discrete joints, continuous-bodied robots have the advantages of flexible bending along the structure and thus strong adaptability in unstructured environments [1]. A continuous-bodied robot can utilize its arm structure as well as its tip. Not only can an end-effector be used for grasping like a traditional robot, but its body can also be considered as a gripping claw, with the entire robot body used to realize the grabbing envelope of objects. Therefore, the robot's task adaptability can be greatly improved. Owing to their unique advantages in task adaptability and obstacle avoidance capability, continuous-bodied robots have gradually become a research focus [1-5].

Continuous-bodied robots can be subdivided into three types: discrete jointed –hyper redundant (including numerous snake-like designs [6-7]), continuum (smooth-bodied with a hard/compliant surface [5]), and soft (deformable body) [8-9]. This paper introduces a novel elephant's trunk robot of the continuum type.

Continuum robots are mainly classified into three categories: tendon-driven continuum robots, continuum robots based on concentric tubes, and fluid-driven continuous robots, as follows:

Tendon-driven continuum robots are remotely actuated, with the main advantages being high load capacity and low backbone mass/profile. Representative examples are prototypes developed by the team at Clemson University [10, 11], the OC Robotics company in the UK [12] researchers at Stanford University [13, 14], and at the Harbin Institute of Technology [15], and the team of [16]. This type of robot operates by remotely actuating tendons connected to a multi-degree-of-freedom backbone core. Correspondingly, the bending of the backbone is achieved by tensioning the tendons.

Continuum robots based on concentric tubes are also remotely actuated, with the key advantages being a small profile and direct actuation of the key shape variables. Representative prototypes were developed and analyzed in [17], [18] and [19-22]. The body of this type of robot is constructed using telescopic tubes, which can translate and rotate with respect to each other. The concentric tube robot is both a skeleton and a power source, and the bending of the robot is achieved by controlling the motion of the tubes.

Fluid-driven continuum robots (pneumatic or hydraulic) form their backbones from their actuators, which act as artificial muscles. The advantages include local control of backbone shape and inherent compliance. Representative examples are the continuum robots developed in [23, 24], the German company Festo [25], and [26, 27-28]. This type of robot uses gas or liquid in closed chambers of the artificial muscles comprising the trunk to modulate the shape of the robot.





Comprehensive research on continuum robots has accomplished important progress [1, 5], particularly in medical applications [3]. And different types of continuum robots have different advantages and disadvantages as shown in Table 1. However, if continuum robots are to be used for more extreme applications, such as space and other challenging environmental tasks, the following deficiencies generally remain:

(a) The problem of extreme environmental adaptability is not yet solved: existing continuum robots driven by fluids, artificial muscles, and many by tendons cannot be used repeatedly in high/low-temperature, vacuum, and high radiation environments in space.

(b) The problem of resource scarcity in remote environments has barely been considered: existing continuum robots are driven by multiple, distributed drive sources, creating a large demand for resources. In addition, if used in outer space and other remote environments, distributed actuation requires special additional thermal control measures, which leads to the incorporation of a considerable number of additional resources.

(c) Inadequacies in the combination of adaptability and ease of control: existing continuum robots require the coordination of multiple segments or sections to achieve bending to adapt to the shape of the object that is being grasped. Therefore, the control and planning process is very complicated. This poses a considerable challenge to the computational capabilities that are suitable for use in extreme environments.

Table 1 Comparison of different types of continuum robots

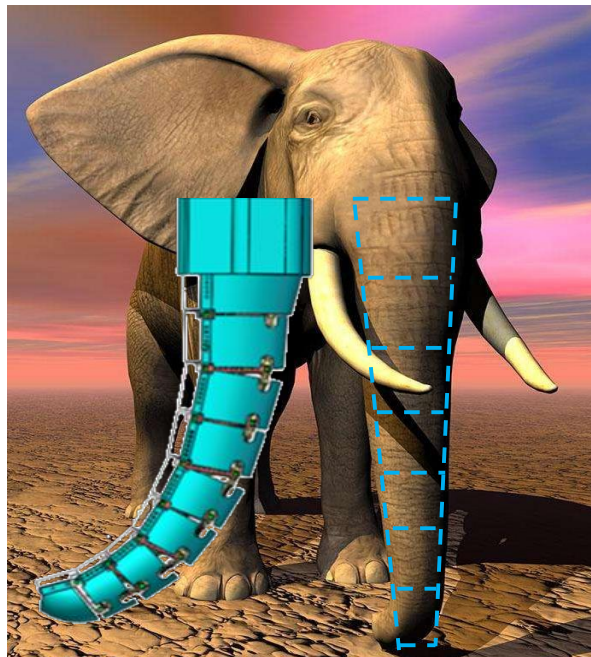
Name	Elephant's Trunk Manipulator [11]	Nitinol tubes [17]	Bionic Handling Assistant [25]	Elephant's Trunk Robot
Type	Backbone-based continuum robots	Continuum robots based on concentric tubes	Fluid-driven continuum robots	Continuous robot driven by a single-motor centralized drive
Working state				
Drive mode	Pull/push the tendon/backbones	Control the motion of the tubes	Pneumatic or hydraulic	A single motor drives multiple units
Advantage	High load capacity	Small profile	Flexibility; inherent compliance	High load capacity; easy control; usage in space environment
Disadvantage	Easy damage due to the fatigue of the tendons	Hard control; low load capacity	Hard control; Weakness of adaptability of extreme environment	Friction between units

To address these problems associated with the use of existing continuum robots in hazardous environments, this paper introduces a new type of continuous robot driven by a single-motor centralized drive. This novel design consists of a series of spatial linkage units connected in series. A single motor drives multiple (all) units. This addresses the contradiction between the required multi-degree of freedom motion and the minimal actuator requirement under strict resource constraints, and the design tradeoff enables biologically inspired capture. In addition, the linkage mechanism is suitable for extreme environments such as in space. The temperature control and protection resource requirements of the relatively fragile, centralized drive system are easily minimized. The proposed new design type is suitable for use in high and low temperature environments, vacuum, high radiation, and in resource-constrained environments in space. The design is introduced and analyzed in the following sections.

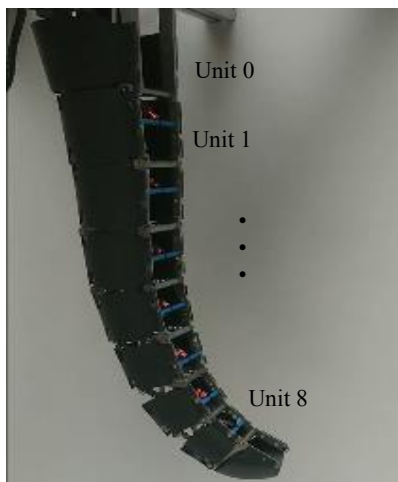
2 SINGLE-MOTOR DRIVEN TRUNK ROBOT DESIGN

The elephant's trunk robot introduced in this study is designed according to the real (biological) elephant's trunk, with the scale reduced. Figure 1(b) is a hard case prototype and Figure 1(c) is a soft case prototype that can be used to accomplish different tasks. The inner part of the trunk robot consists of nine link mechanisms of the same design and of successively reduced size. All the link mechanism units are driven by the same motor via a scissors mechanism, and each link unit transmits power through the scissors' connecting rod. A telescopic spring is arranged inside each link mechanism unit to maintain the

shape of the robot and assist the reset action after the completion of the work. The main parameters of the trunk robot are shown in Table 2.



(a)



(b)



(c)

Fig. 1 Elephant's trunk robot: (a) dimensions, (b) hard shell, and (c) soft shell

The designed elephant's trunk robot contains nine units, including one base unit and eight actuation units. There is only one motor drive in the entire robot, i.e., all nine units are driven by the same motor. In the single-motor drive operation, nine units can complete in-plane bending and stretching actions so that the robot can hold a wide range of objects. By installing a detection device at the end of the robot, the trunk robot can perform monitoring and detection functions in a given environment. In addition, if a rotary joint is installed at the base unit, the robot can realize the bending motion in the three-dimensional space, greatly improving the adjustment capability of the mechanism.

Table 2. Parameters of the robot

Parameter	Value
Length (cm)	78
Diameter (cm)	50-125
Weight (Kg)	3.78
Unit Number	9
Motor Number	1

There are some parameters compared to other similar robots in Table 2. The designed robot has a comparatively smaller base area and weight, so it has better flexibility and larger load bearing capacity. The robot is only driven by a single motor, which greatly saves the drive energy of the entire robot system. At the same time, the robot has a large elongation length, and thus has a more desirable capture range.

The designed trunk robot has the following features:

Feature A: Multiple motion units are driven by a single motor

Unlike previously proposed trunk robots [29-32], the core component of the trunk robot designed in this study is a modular unit consisting of a link mechanism and a telescopic spring. All of the designed action unit mechanisms have the same core design. In principle, an infinite number of actuation units can be connected end-to-end to form an infinite-degree of freedom elephant trunk robot driven by a single motor arranged at the base, as suggested in Fig. 2. A single motor drives a plurality of actuation units connected in series, and as long as the motor driving force is sufficiently large, or the action unit mass and friction of the motion pair are sufficiently small, the elephant's trunk robot can perform bending and stretching actions with a single actuator.

In principle, while there could be infinite number of units, considering realistic friction and deformation issues, in order to approach the shape and size of an elephant's trunk in a practical way, the prototype of the elephant's trunk robot presented in this paper contains eight actuation units and one base unit.

The fact that a single motor drives the linkage of multiple units simplifies the requirements of the sensor and control systems during the robot operation. Existing continuum and elephant's trunk robots are generally based on multimodal sensing, planning, and control, which requires multiple motor/drivers to drive the robot's body mechanism to allow it to bend and eventually envelop the target object. Compared to previous work, the robot proposed in this paper exploits its novel mechanism instead of requiring a multi-actuator linkage to realize the bending function to adapt to the target object.

A single motor drive also reduces resource requirements. The sole drive motor is located at the base unit, and all the actuation units distal to it are designed as lightweight space link mechanisms, reducing the burden on the weight of the elephant's trunk robot. In addition, the size at the base is very small, which facilitates the integration of the elephant's trunk robot with other motion platforms, and further realizes an abundance of additional functions in an easier manner.

Feature B: Strong adaptability

The elephant's trunk robot introduced herein has increased adaptability capabilities in three key aspects: it can grasp a wide range of different shapes and sizes, it can hold that grasp at different positions, and it can perform these operations in a variety of extreme environments, as discussed below.

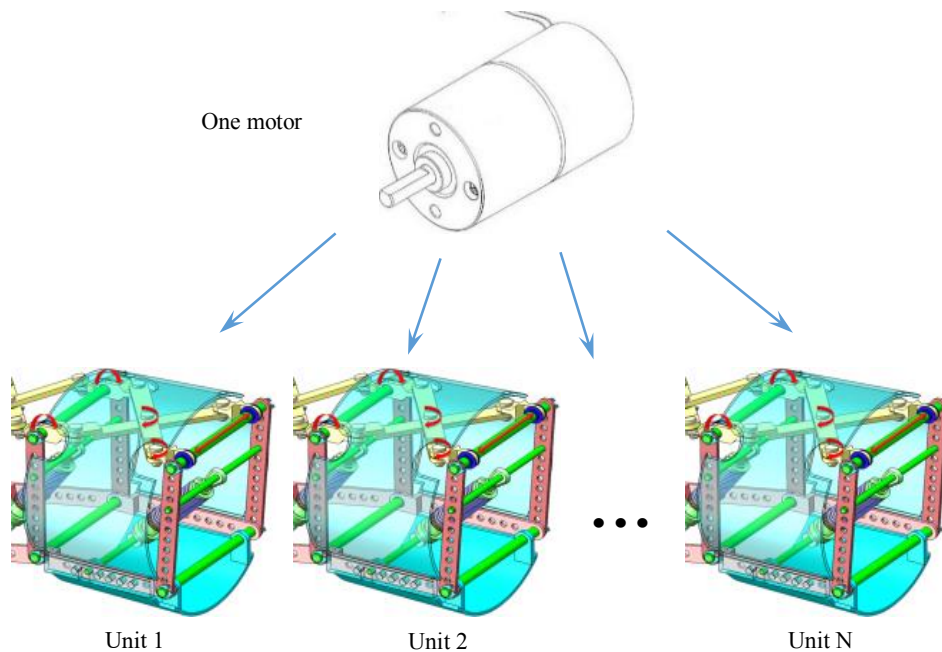


Fig. 2 Driving principle: All units are driven by the same motor

Adaptability 1: Target adaptability to different shapes and sizes

The action unit module designed for the robot consists of a spatial linkage mechanism and a spring. It has one degree-of-freedom. If the elephant's trunk robot contains N actuation units, the robot has N degrees of freedom, but the robot has only one motor drive. In this way, the overall robot body is an under-actuated mechanism. When holding a target object, the elephant's trunk robot completely envelops the target in a whole-arm grasp. The final shape of the robot is determined by the shape and size of the target being grasped, as shown in Fig. 3. Note that the robot has the advantage of completing the capture as a function of its mechanism, i.e. without the need for determining a priori the exact shape and location of the target.

Adaptability 2: Adaptability to targets at different locations

In addition to holding objects of different shapes and sizes, the elephant's trunk robot can hold these objects at different positions and achieve the final complete envelope. As long as the relative position and size are within the allowable range, when the elephant's trunk robot holds a fixed object that cannot move, it can adapt to the position of the affected object and capture the target at different positions, as shown in Fig. 4.

Adaptability 3: Suitable for different hazardous environments

The elephant's trunk robot designed in this study consists of a base and a multistage linkage mechanism. The only drive motor used is placed in the base.

The connecting rod mechanism has excellent environmental adaptability. As long as a suitable material is selected, the connecting rod mechanism can be applied to dangerous environments, such as when exposed to extreme corrosion, extremely high temperature, strong radiation, and in other similar cases. Compared with the soft body material of many previously proposed continuum trunk robots, the link mechanism has obvious advantages. In addition, the power transmission between the units of the trunk robot is realized by connecting rods instead of tendons or artificial muscles, and it can be effectively applied in long-term and extremely high/low temperature environments, giving a significant advantage in

reliability and service life. In the trunk robot introduced here, the only sensitive core component, the driving motor, can be safely enclosed in the base and relatively easily protected.

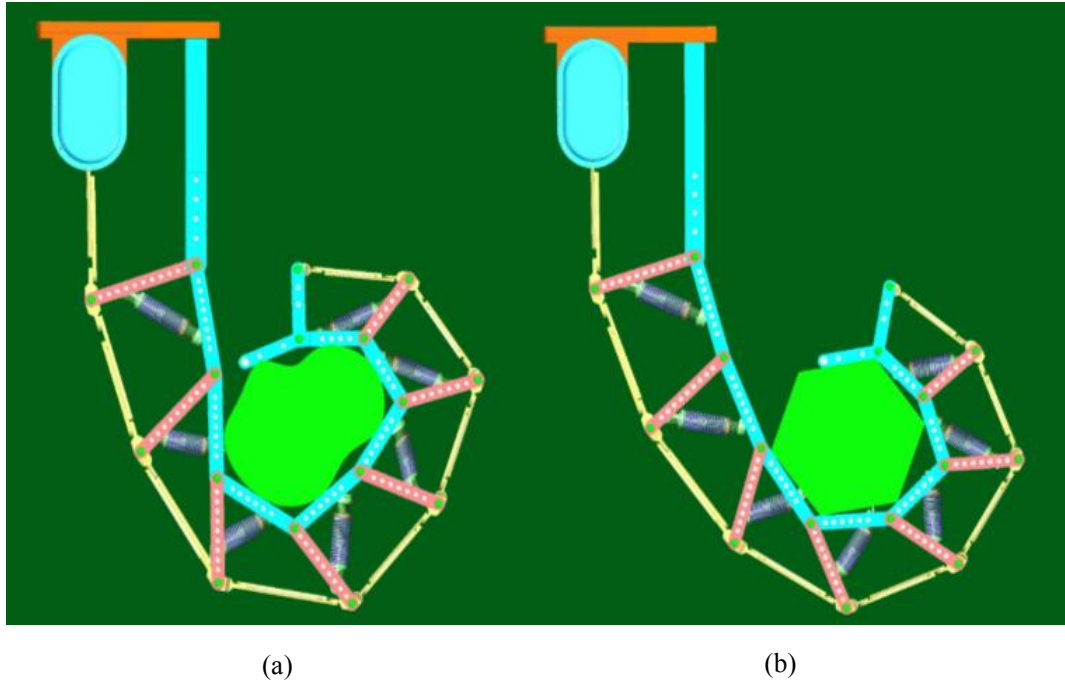


Fig. 3 Robot grasps objects of different shapes and sizes: (a) holding irregularly shaped objects, and (b) holding polygonal objects

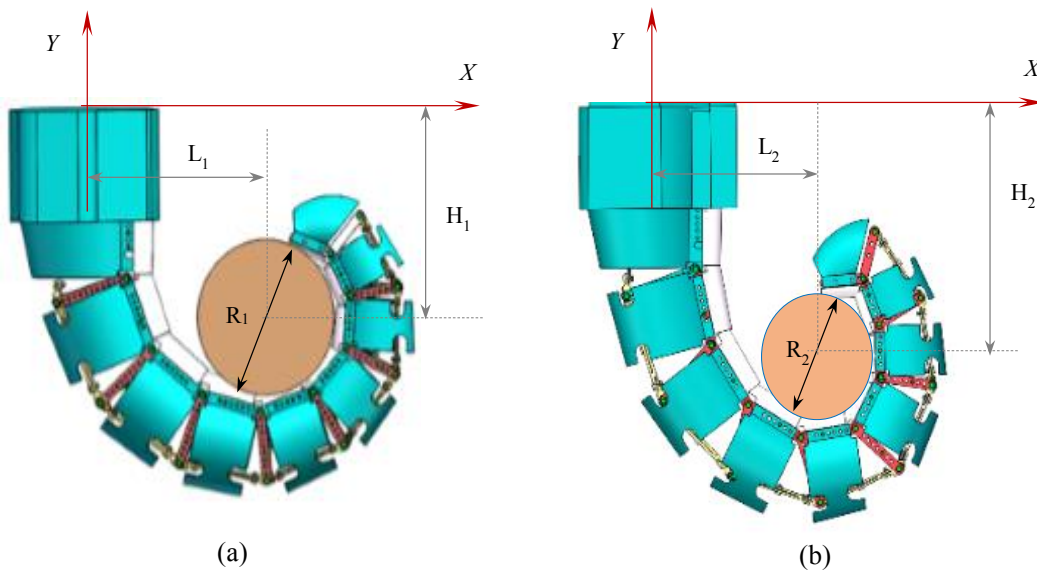


Fig. 4 Robot grasps objects at different positions: (a) holding a proximal target, and (b) holding a closer target

Also, with the trunk robot having only one motor, this is associated with a low energy consumption and high reliability, and in this sense is highly suitable for extremely hazardous environments, such as in outer space and in nuclear industries, where resource constraints are significant.

Feature C: Clear robot advantages in capturing non-cooperative targets in space

At present, the established procedure for capturing non-cooperative targets (satellites, space debris, etc.) in space is based on point-to-point capture. This type of capture system is mainly based on a traditional robot arm and a terminal gripper [33]. When carrying out the capture mission, the robotic arm must move the gripper to the target. It can be observed that this current mode of capture method makes it difficult to achieve an effective capture of rotating non-cooperative targets, as the precision of the robot arm is negated by the uncontrolled movement of the target, and precise relative station keeping is required. Thus the point capture methodology places very high demands on the performance of the target measurement system and the capturing vehicle controller.

The elephant's trunk robot presented here not only offers the option of grasping by the robot's end effector as with a traditional robot, but also a new and more adaptive mode of compliant whole arm grasping of the target's envelope through the robot's own compliant body structure. The new capture system expands the current point-to-point capture method to a large-scale capture method. The capture scale is associated with a qualitative fly-through, enabling direct capture of non-cooperative targets, such as spin/roll, as shown in Fig. 5. While improving the capture efficiency and success rate, the requirements for auxiliary systems, such as measurement and precise station-keeping systems, have been greatly reduced.

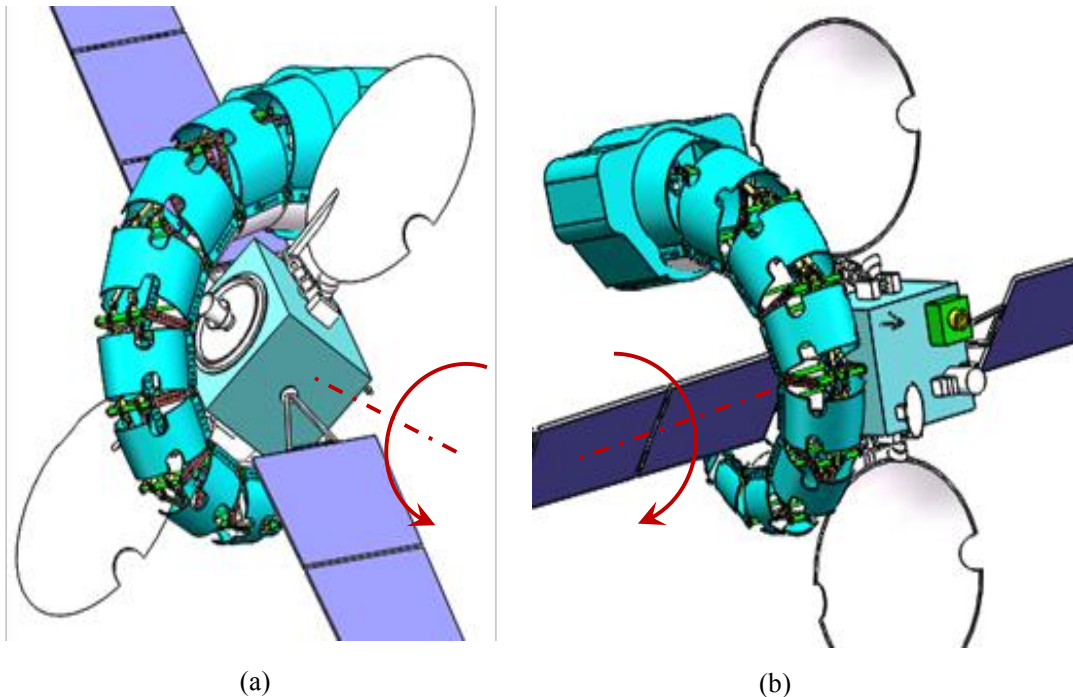


Fig. 5 Robot used in space extreme environments: (a) holding a satellite body that rotates around an isometric axis and (b) holding a satellite solar windsurfer that rotates around a central axis (Size parameters can be designed according to the specific needs of the space application)

3 MECHANISM PROTOTYPE AND ANALYSIS

Based on the link mechanism concept, we next describe the physical realization of the motion unit, the single motor drive, and the motion characteristics and bending motion of the resulting elephant's trunk robot hardware driven by a single motor.

Principle of robot mechanism

As noted previously, the trunk robot consists of multiple units, and each unit is composed of a space link mechanism and a spring, as shown in Fig. 6.

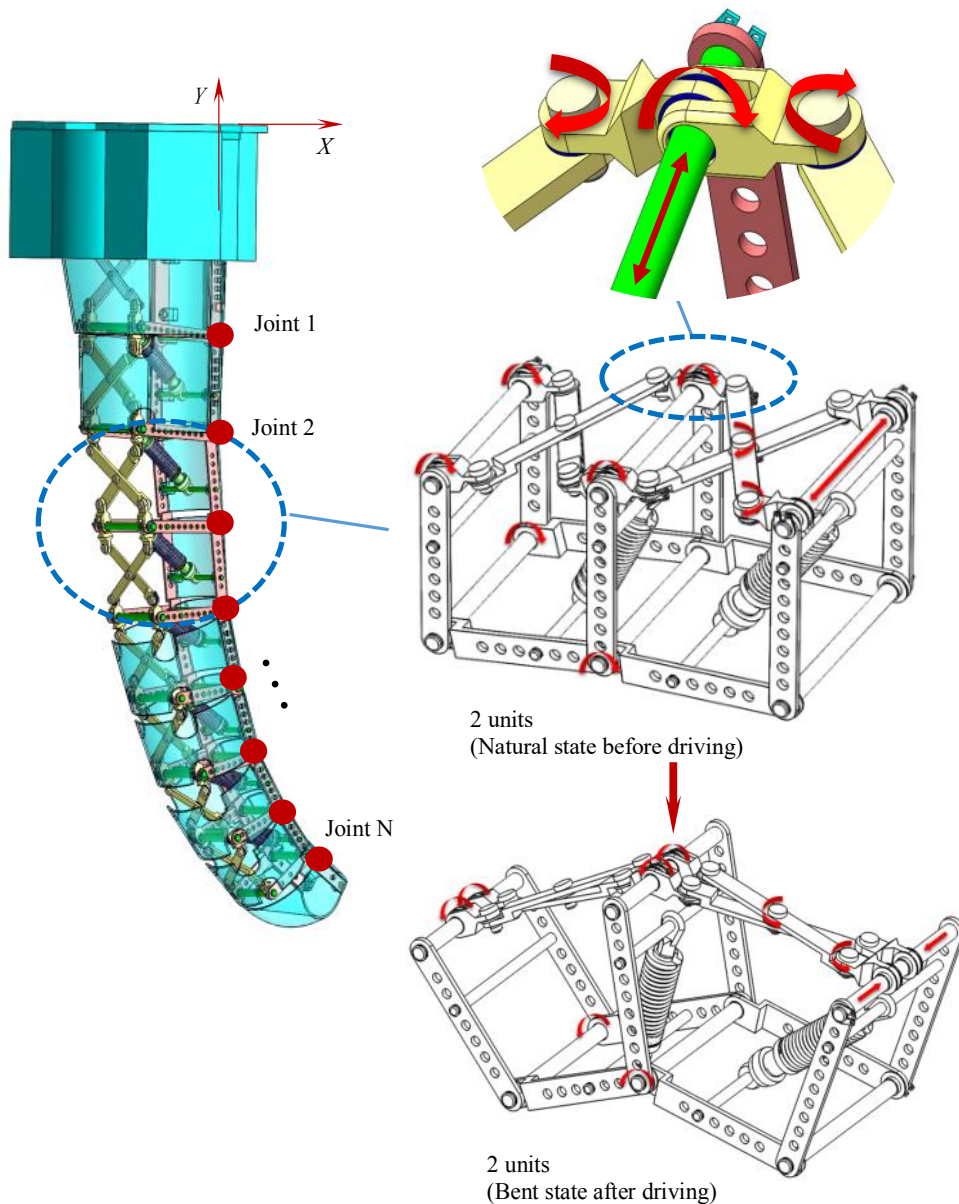


Fig. 6 Mechanical design of the core robot units

Each unit of the trunk robot is itself an under-actuated mechanism. The under-actuated unit is formed by coupling a scissors mechanism, a connecting rod, and a spring. Different from commonly used under-actuated mechanisms, the under-actuated mechanism unit proposed in this work holds a target object and ensures that all the joints move synchronously towards the target under the driving of the scissors mechanism, thereby significantly shortening the time for grasping the object.

The key part of each unit is the scissors mechanism. The scissors mechanism is responsible for the telescopic and rotational motion of the unit. Compared with traditional scissors mechanisms, this design adds a rotation pair to the connecting end of the connecting rod so that the scissors mechanism not only can achieve telescopic motion in the plane, but can also realize rotation of the scissors mechanism itself about an axis perpendicular to that plane. In this way, the bending of the trunk robot is realized. In addition, the length of the input end of the scissors lever is greater than the length of the output end. According to the principle of the lever, the designed scissors mechanism can thereby realize a torque amplification function.

As shown in Figs. 6 and 7, when the scissors mechanism is driven, the supporting linkage will be driven at the same time. The supporting and bottom linkages are connected by a spring device. In the no-load case, the spring force is greater than the friction between the supporting and bottom linkages, which can then be regarded as a rigid connection. Thus, the two linkages move together, and the other units perform the same movement.

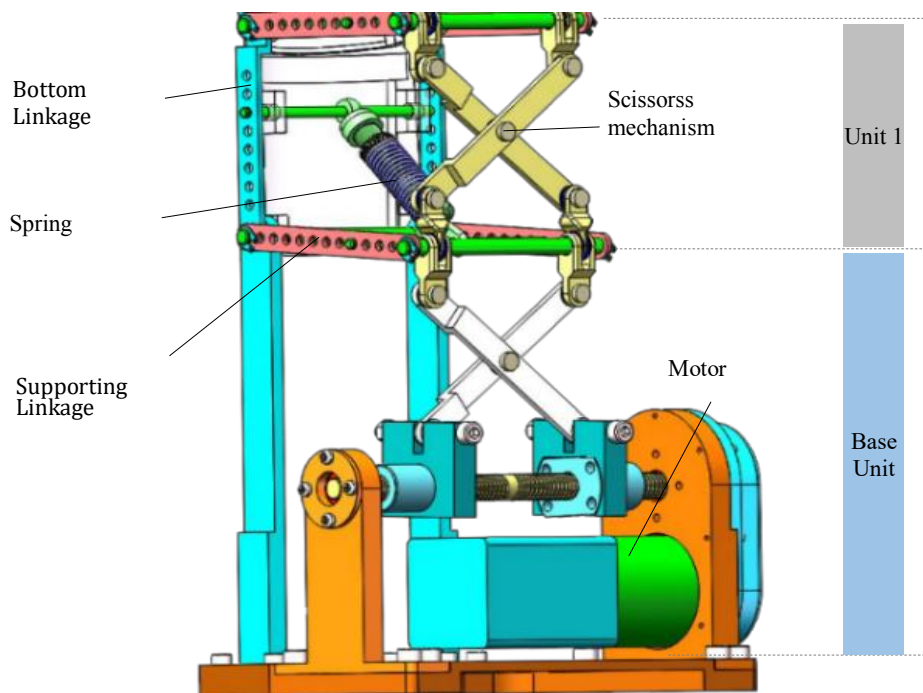


Fig. 7 Mechanical design of the base unit and unit 1

As shown in Fig. 7, in the base unit, the motor is mounted on a fixed base, and a screw is driven to rotate through a gear transmission. The screw is a screw nut with positive and negative directions. Therefore, the rotation of the screw will cause the nut to synchronously move in the opposite direction, driving the scissors mechanism in the base unit to perform the telescopic movement, and then driving the scissors mechanism of unit 1 to transfer it step-by-step to realize the bending motion of the elephant's trunk robot.

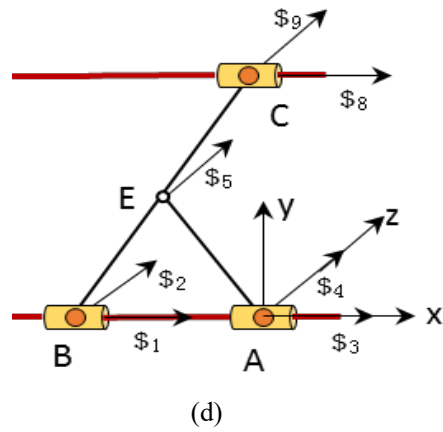
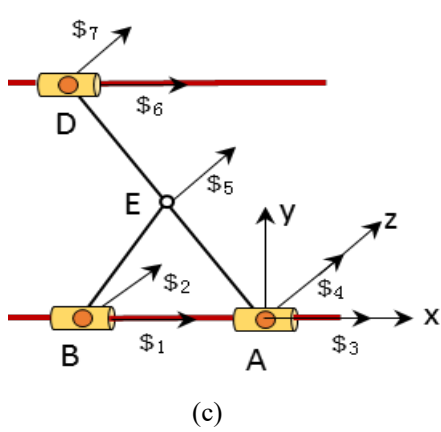
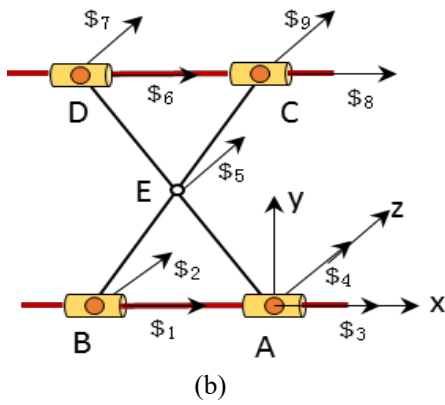
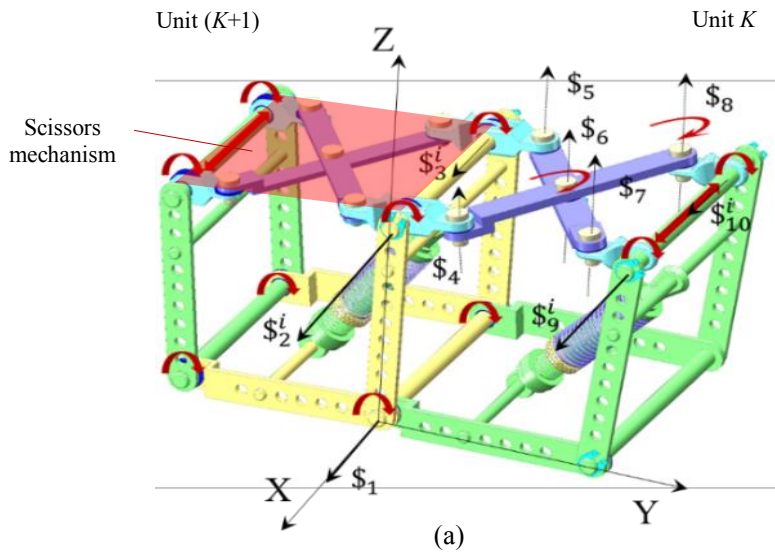


Fig. 8 Schematics of the kinematic unit and motion pair–screw coordinate system: (a) two-unit schematic, (b) scissors mechanism, (c) left part of the scissors mechanism, and (d) right part of the scissors mechanism

Freedom and movement characteristics

The following analysis is performed by using the constraint between the various connecting rods of the trunk robot in accordance to the theory of screws, followed by an analysis of the motion characteristics of the trunk robot.

The trunk robot is composed of a plurality of units all with the same working principles and design, so that just one of the units is analyzed in this study. Because each unit is an under-drive structure, the mechanism itself can perform corresponding self-transitions according to encountering different objects to adapt to stable holding configurations of different objects. The movement of the robot body before and after its own transformation is controllable. This work considers the robot's state before grabbing an obstacle and analyzes it.

As shown in Fig. 8, the corresponding spiral movement is marked on the unit. Before contact with an object, the support and bottom links are all brought closer to the object under the action of the spring. Therefore, the support and the bottom links can be regarded as rigid connections, and are considered as the same component.

In order to analyze the mechanism that underlies the movement of the unit, a unit of the transmission's partial scissors mechanism is first analyzed. Owing to the special nature of the scissors mechanism, the coordinates of all the rotating hinges in the mechanism are in the same plane. Analysis is conducted in the plane where the scissors mechanism defines. At this time, the case relevant to the cylindrical pair is equivalent to the case where the pair is moved. We establish a coordinate system, as shown in figure 8, so that the coordinates of point A are $(0, 0, 0)$ and the coordinates of point B are $(b_x, 0, 0)$, E-point coordinates are $(e_x, e_y, 0)$, D-point coordinates are $(d_x, d_y, 0)$, and C-point coordinates are $(c_x, c_y, 0)$. Since the five points are all in the same plane, the X-shaped pair can be regarded as a rotation pair perpendicular to this plane.

The screw of the rotating pair and the screw of the pair in the plane [34] are:

$$\begin{aligned}
 \$_1 &= [0, 0, 0, 1, 0, 0]^T \\
 \$_2 &= [0, 0, 1, -b_x, 0, 0]^T \\
 \$_3 &= [0, 0, 0, 1, 0, 0]^T \\
 \$_4 &= [0, 0, 1, 0, 0, 0]^T \\
 \$_5 &= [0, 0, 1, -e_x, e_y, 0]^T \\
 \$_6 &= [0, 0, 0, 1, 0, 0]^T \\
 \$_7 &= [0, 0, 1, -d_x, d_y, 0]^T \\
 \$_8 &= [0, 0, 0, 1, 0, 0]^T \\
 \$_9 &= [0, 0, 1, 0, p_y, 0]^T
 \end{aligned} \tag{1}$$

The two interconnected branches in Fig. 8(b) are split into two parts in (c) and (d). AD and BC are the two links of the scissors mechanism. Rod BC is considered as the output component of the lower closed-loop system (as shown in fig. 8(b)). Additionally, the constraint screws of the two branches $\{\$, \$_2\}$ and $\{\$, \$_4, \$_5\}$ on BC are:

$$\{\mathcal{S}_1, \mathcal{S}_2\}: \begin{cases} \mathcal{S}_{a1}^r = [0, 0, 0, 1, 0, 0]^T \\ \mathcal{S}_{a2}^r = [0, 0, 0, 0, 1, 0]^T \\ \mathcal{S}_{a3}^r = [0, 0, 1, 0, 0, 0]^T \\ \mathcal{S}_{a4}^r = [0, 1, 0, 0, 0, 0]^T \end{cases} \quad (2)$$

$$\{\mathcal{S}_3, \mathcal{S}_4, \mathcal{S}_5\}: \begin{cases} \mathcal{S}_{b1}^r = [0, 0, 0, 1, 0, 0]^T \\ \mathcal{S}_{b2}^r = [0, 0, 0, 0, 1, 0]^T \\ \mathcal{S}_{b3}^r = [0, 0, 1, 0, 0, 0]^T \\ \mathcal{S}_{b4}^r = \begin{bmatrix} e_y \\ e_x \end{bmatrix}, 1, 0, 0, 0, 0 \end{cases}^T \quad (3)$$

It can be found that the reciprocal screw of the BC component is $\{\mathcal{S}_{a1}^r, \mathcal{S}_{a2}^r, \mathcal{S}_{a3}^r, \mathcal{S}_{a4}^r, \mathcal{S}_{b4}^r\}$. Rod BC's permissible motion screw can be obtained by the secondary screw of this reciprocal screw system.

$$\mathcal{S}_{BC}^{rr} = [0, 0, 1, 0, 0, 0]^T \quad (4)$$

It can be observed from this equation that the movement of rod BC is limited to a rotation around the Z axis. In the same way, the AD rod is output as a component, and the same conclusion can be obtained.

Further analysis shows that the rotation of rod BC about the Z axis can be decomposed into a composite movement along the X- and the Y-axes. The movement along the Y-axis is the driving force of the next unit of the trunk robot driven by the scissors mechanism because each scissors mechanism is connected to the support link of the subsequent unit through the slide shaft. The support link and the bottom link are connected through the rotation pair. Thus, the support link can only rotate about the rotation axis where the two are located. The bending motion of each unit of the trunk robot is also caused by the rotational movement of the support link. In addition, the rotation of the support link will in turn drive the bending of the scissors mechanism. The cylindrical pair at the connection of the head and tail of the proposed scissors mechanism of the trunk robot guarantees that the scissors mechanism will perform bending movements about the support link. Therefore, the entire robot will also realize its bending motion when it approaches the target.

From the reciprocal screw of equation (4), it can be seen that M is an infinitely constrained binding couple that restricts the rotation about the Y-axis. The same constraint is applied to the rods connected to each motion screw, i.e., each component loses the freedom to rotate about the Y-axis, and there is only one common constraint.

According to the revised G–K formula [34]:

$$M = d(n - g - 1) + \sum_{i=1}^g f_i + v - \zeta \quad (5)$$

In the formula listed above, M represents the degrees-of-freedom of the mechanism, n represents the number of components including the frame, g represents the number of motion pairs, f_i represents the degrees-of-freedom of the i^{th} motion pair, d represents the level of the mechanism — also referred to as the common constraint factor — v represents the number of redundant constraints, which is equal to the number of independent redundant constraints after removing the factors of the common λ constraints, and ζ is the number of the local degrees-of-freedom. Owing to the number of over-constraints, $v=3$. Additionally, $d = 6 - \lambda$, whereby in this study $\lambda = 1$. Thus, $d = 6 - \lambda = 5$, $n = 8$, and $g = 10$.

Considering the supporting link of the robot as an output target, the freedom of movement of the cylindrical pair in the scissors mechanism along the X direction is the local freedom of the robot, and does not affect the movement of the output member. That is, it includes a partial degree-of-freedom, so $\zeta = 1$. Substituting the upper number into the corrected DOF expression yields,

$$M = d(n - g - 1) + \sum_{i=1}^g f_i + v - \zeta = 5(8 - 10 - 1) + 14 + 3 - 1 = 1 \quad (6)$$

Therefore, each robot unit has a single degree-of-freedom, and when the bottom link of the robot is touching an obstacle, contact is ensured by compressing the spring between the support and the bottom links. The continuous motion of the scissors mechanism realizes the complete grasping of a target object by the robot.

For a trunk robot with N units arranged serially, there are N-degrees of freedom, as shown in Fig. 6. However, unlike a fully-driven, single-chain robot system, the N degrees-of-freedom are not always used during the movement of the robot. When no obstacle or object is touched, each joint is locked in accordance to the effect of its own dynamic spring-restraint. Once the movement of the mechanism is suddenly blocked, the driving force overcomes the dynamic constraint automatically. The corresponding degree-of-freedom is lost [24], and self-organization of objects of different shapes is achieved.

As shown in Fig. 9, the bending process of the trunk robot can be summarized as follows: when the scissors mechanism is extended, the support links are driven to move together, and the support and bottom links are connected by a spring device. In the no-load case, the spring force is greater than the friction between the bottom link and the support link. In this case, there is no relative movement between the support link and the link at the bottom part, which can be regarded as a rigid connection. Therefore, the support link will rotate together with the bottom link and the other units will perform similar movements. Before the trunk robot comes into contact with a target object, the entire trunk robot will move closer to the target object under the drive of the scissors mechanism.

When a unit touches an obstacle or a target object, the bottom link that is in contact with it will not move. When the shear force continues to increase, it will be greater than the spring force between the support link and the bottom link. Relative rotation will occur by compressing the spring device between the support link and the link at the bottom part, thereby ensuring the continued movement of the scissors mechanism. This leads to the continued movement of the other joints to the target object, finally achieving the complete enveloping of the target object.

4 SPRING PARAMETER ANALYSIS AND DESIGN

The springs are a very important part of the design. Their parameters and arrangement directly affect the movement of the trunk robot. We next analyze and design the spring parameters and provide reference for the subsequent model design. The connecting rod at the bottom element and the supporting connecting rod of each unit have mounting holes for adjusting the position of the springs. Different movement trajectory curves can be obtained by adjusting (a priori) the position of the spring. Fig. 10(a) shows the initial positions of units K and (K+1) when different spring parameters and layouts are selected. The corresponding trajectory curves of the entire trunk robot are shown in Fig. 10(b) and Fig. 10(c).

Each unit of the trunk robot has the same design, but the dimensions (scales) are slightly different. The springs inside each unit have similar effects on the movement of the unit. Herein, unit 1 was selected as an example for analysis. The contact force between the unit and the target is F , and the direction is always perpendicular to BD. The stiffness coefficient of the spring is k . Points A, B, and C are the three joints of the internal linking mechanism of unit 1. Correspondingly, E and G are the fixed points at the end of the spring, and point C is the point of the load. The length of BG is l_1 , the length of BE is l_2 , the

variable length of spring is l_3 (related to F), the length of BC is l_4 , and $\angle EGB = \theta_t$. In the free state, the length of the spring is l_{30} .

When the motion unit is in equilibrium during the adaptation process, the following relationship applies

$$\begin{cases} F = \frac{k(l_{30} - l_3)l_1 \sin \theta_t}{l_4} \\ \cos \theta_t = \frac{l_1^2 + l_3^2 - l_2^2}{2l_1 l_3} \end{cases} \quad (7)$$

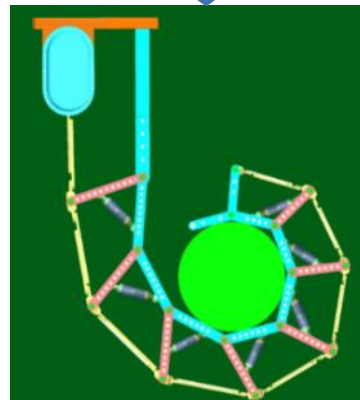
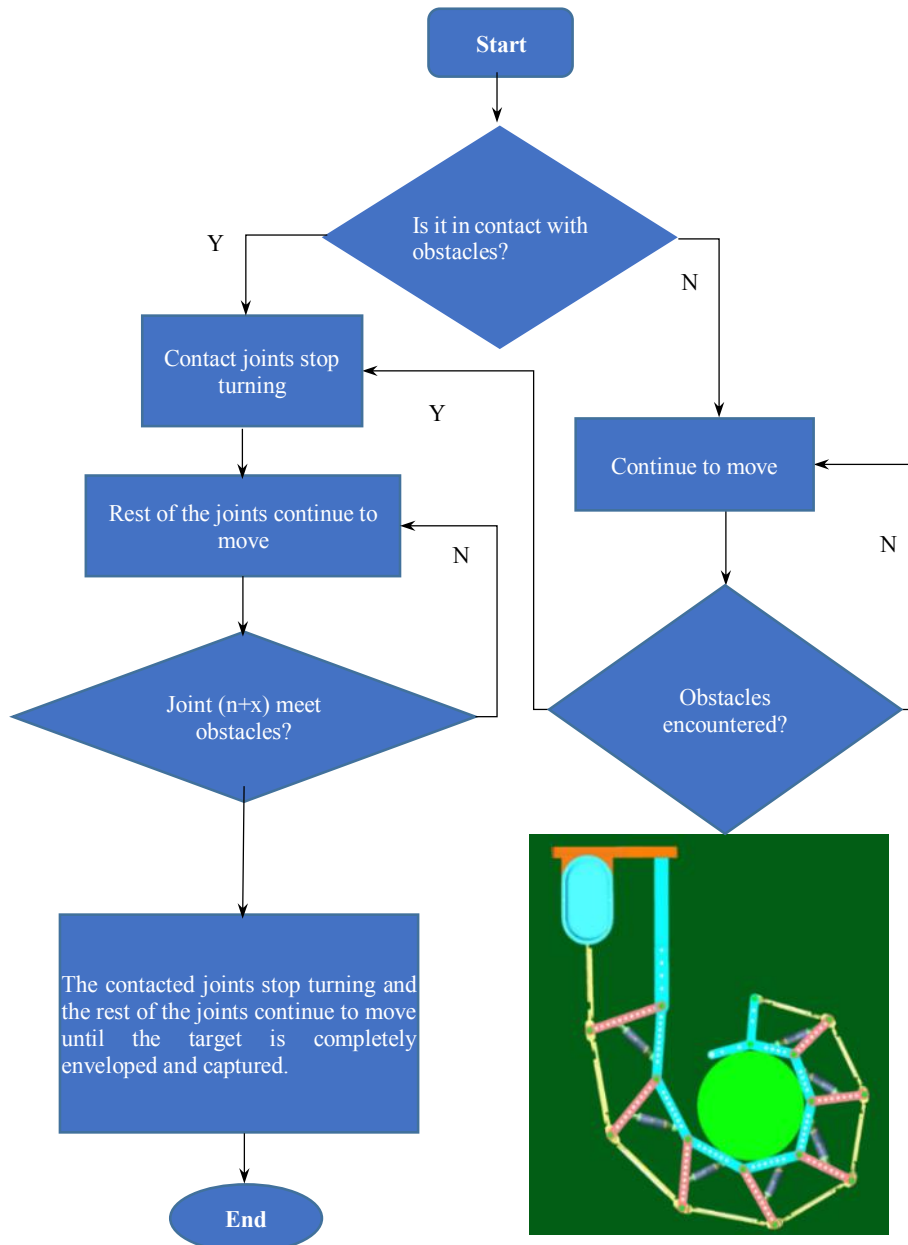


Fig. 9 Elephant's trunk robot flowchart

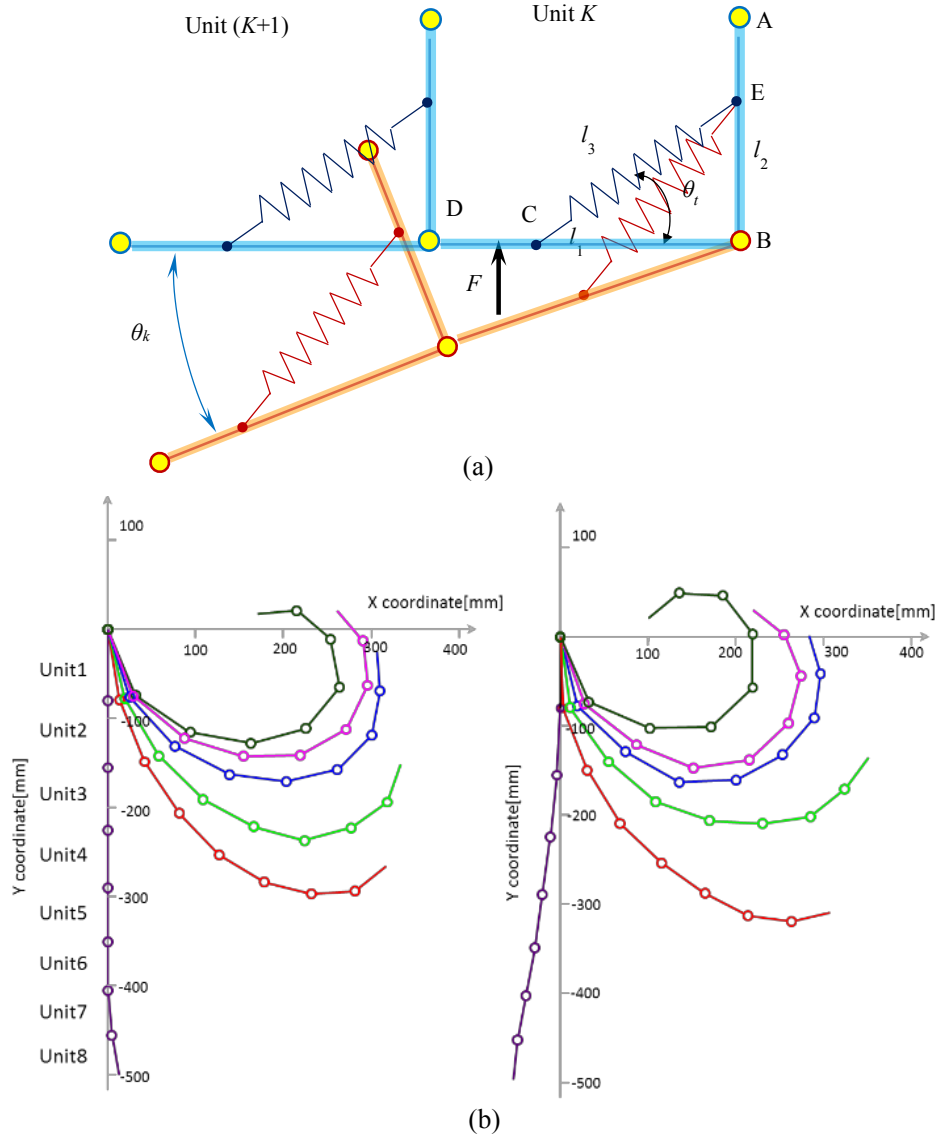


Fig. 10 (a) Initial angle of unit k and unit $(K+1)$ with different positions of the spring, (b) trajectory of the robot with different positions of spring

The relationship between the available stiffness k and the force F is

$$k = \frac{l_4 F}{l_1 (l_{30} - l_3) \left[1 - \left(\frac{l_1^2 + l_3^2 - l_2^2}{2l_1 l_3} \right)^2 \right]^{1/2}} \quad (8)$$

Based on measurements of the physical system $l_{30} = 60\text{mm}$, $AB = 80\text{mm}$, and $BD = 70\text{mm}$. The length of BC is 50mm , the length of l_3 is 50mm , and the spring rates are 10N/mm , 17N/mm , 25N/mm , and 30N/mm , respectively. Equ. (7) can be used to derive the relationship between the load and the spring stiffness coefficient, and the $F-k$ curve can be obtained after the relevant data are entered, as shown in

Fig. 11. As it can be observed from Fig. 11, there is a linear relationship between force F and the spring stiffness coefficient k . When the force is set to the same value, the greater the distance is between the force contact point and the hinge point, the greater is the required stiffness coefficient of the spring. When the angle is 1.6 rad after calculation, the change rate of the spring stiffness is zero, and the required spring stiffness is minimized, so the optimal angle during operation is approximately 1.6 rad.

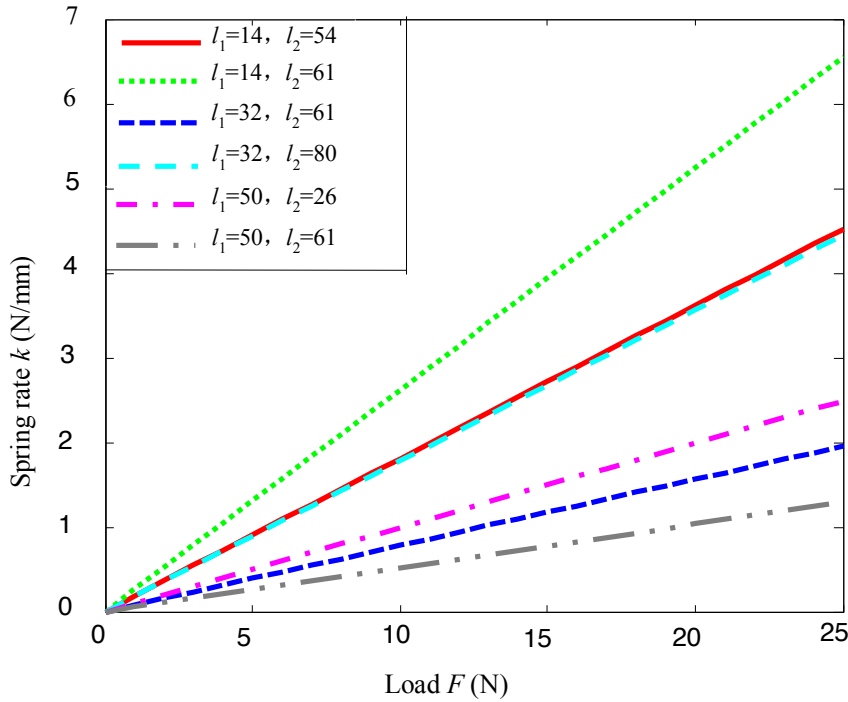
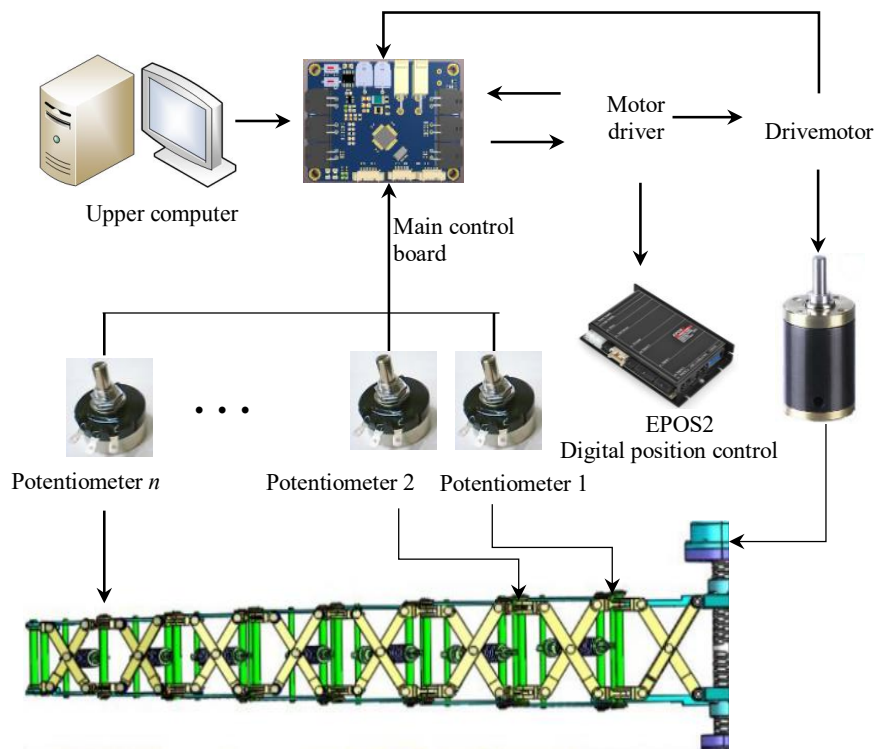


Fig. 11 F-k curve: Relationship between the force and the stiffness coefficient of the spring

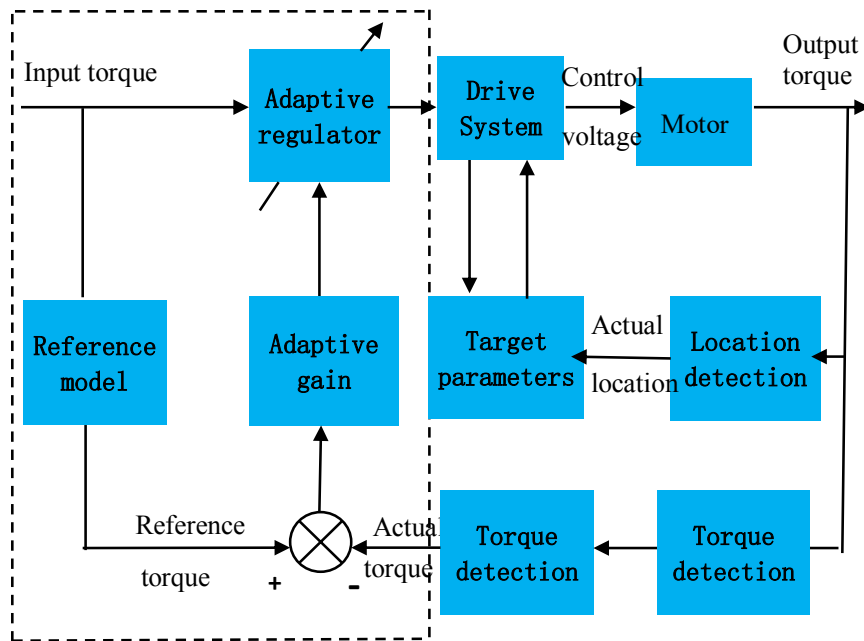
5 CONTROL SYSTEM DESIGN

The model of the developed control system is shown in Fig. 12. The hardware of the system consists of a control circuit, a motor drive circuit, and a torque measurement circuit. In the dashed box is a Model Reference Adaptive Controller (MRAC). The error between the first reference torque and the actual torque is transmitted to the adaptive regulator via the adaptive gain, where the actual torque is obtained by the voltage detection. The adaptive regulator then calculates the control torque based on the input torque and the adaptive gain, and finally drives the holding mechanism to achieve the holding motion.

An angle measuring device needs to be included in the unit nodes. We use potentiometers, which are common angle detection devices, and are widely used in robotic unit angle measurements. Resistances of the potentiometers are increased when the elephant trunk robot moves closer to the object. The unit stops rotating and the resistances are stable at a constant value when touching an obstacle. Finally, resistances of group of the potentiometers stabilize at constant values when the object is completely grasped. Angles of units are received by CAN-Bus messages in an embedded operating system to achieve dynamic real-time response of the trunk robot, which can easily provide the required motion state of each unit.



(a)



(b)

Fig. 12 Control system diagram of the robot: (a) system composition, and (b) control system model

6 ROBOT FORWARD KINEMATICS

For the geometric parameters of the given member of the robot and the displacement of the joint, the pose of the end link coordinate system relative to the base coordinate system is solved, and the coordinate systems of the pseudo nose robot are established, as shown in Fig. 13.

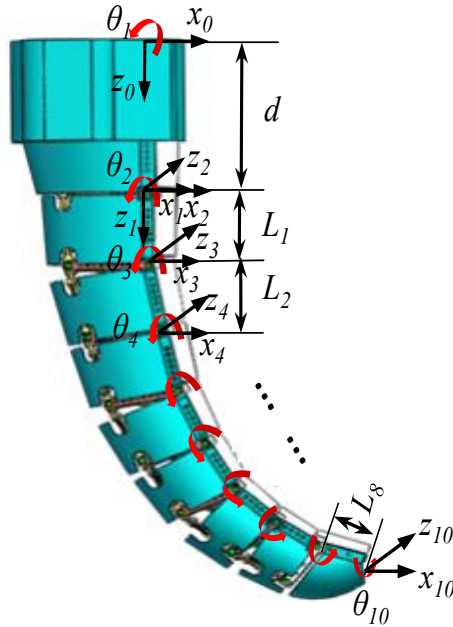


Fig. 13 DH coordinate system of elephant's trunk robot

The DH coordinate system is established for each unit of the elephant's trunk robot, as shown in Fig. 13, and parameter table of the DH corresponding system is obtained, as shown in Table 3. The number of elephant's trunk robot units analyzed here is 10, and the robot is mounted on a rotating platform.

Table 3. Parameters of DH coordinate system of elephant's trunk robot

No.	Rotation angle α_{i-1}	Rod length a_{i-1}	Offset d_i	Joint angle θ_i
1	0°	0	d	θ_1
2	-90°	0	0	θ_2
3	0°	L_1	0	θ_3
4	0°	L_2	0	θ_4
5	0°	L_3	0	θ_5
6	0°	L_4	0	θ_6
7	0°	L_5	0	θ_7
8	0°	L_6	0	θ_8
9	0°	L_7	0	θ_9
10	0°	L_8	0	θ_{10}

According to the transformation matrix based on coordinates

$${}^{i-1}P = {}^{i-1}T_R {}^R T_\theta {}^\theta T_P {}^P T_i {}^i T^i P = {}^{i-1}T^i P \quad (9)$$

$${}^{i-1}T^i = \begin{bmatrix} c\theta_i & -s\theta_i & 0 & a_{i-1} \\ s\theta_i c\alpha_{i-1} & c\theta_i c\alpha_{i-1} & -s\alpha_{i-1} & -s\alpha_{i-1} d_i \\ s\theta_i s\alpha_{i-1} & c\theta_i s\alpha_{i-1} & c\alpha_{i-1} & c\alpha_{i-1} d_i \\ 0 & 0 & 0 & 1 \end{bmatrix} \quad (10)$$

where, $c\theta_i = \cos \theta_i$; $c\theta_{i-1} = \cos \theta_{i-1}$; $s\theta_i = \sin \theta_i$; $s\theta_{i-1} = \sin \theta_{i-1}$;

The change matrix of the end joint of the elephant trunk robot relative to the base coordinate system is as following,

$${}^0T_n = {}^0T_1(\theta_1) \cdot {}^1T_2(\theta_2) \cdot {}^2T_3(\theta_3) \cdots {}^{n-1}T_n(\theta_n) \quad (11)$$

In summary, the kinematic equation of the end of the elephant's trunk robot is obtained,

$$\begin{aligned} P_x &= L_1 c_{12} + L_2 c_{123} + L_3 c_{1234} + L_4 c_{12345} + L_5 c_{123456} + L_6 c_{1234567} + L_7 c_{12345678} + L_8 c_{123456789} \\ P_y &= L_1 s_{12} + L_2 s_{123} + L_3 s_{1234} + L_4 s_{12345} + L_5 s_{123456} + L_6 s_{1234567} + L_7 s_{12345678} + L_8 s_{123456789} \\ P_z &= d \end{aligned} \quad (12)$$

where, $s\theta_{123\dots n}$ and $c\theta_{123\dots n}$ are the sine and cosine of the sum of n joint angles,

$$\begin{aligned} s\theta_{123\dots n} &= \sin(\theta_1 + \theta_2 + \theta_3 + \dots + \theta_n) \\ c\theta_{123\dots n} &= \cos(\theta_1 + \theta_2 + \theta_3 + \dots + \theta_n) \end{aligned} \quad (13)$$

WORK SPACE

The work space of the elephant's trunk robot is the key to its ability to accomplish the expected task. Therefore, based on the forward kinematics analysis, the Monte Carlo method is used to analyze the robot's motion space.

(1) The kinematics of the elephant's trunk robot is solved, and then the position vector of the robot end position in the base coordinate system can be obtained;

(2) Using the Rand() function to generate a series of random numbers [0,1], which can be used to form random numbers of each unit variable.

$$\theta_i = \theta_i^{\min} + (\theta_i^{\max} - \theta_i^{\min}) \times \text{Rand}(N,1) \quad (14)$$

where, θ_i^{\min} is the minimum range of rotation of the joint i and θ_i^{\max} is the maximum range of rotation of the joint i.

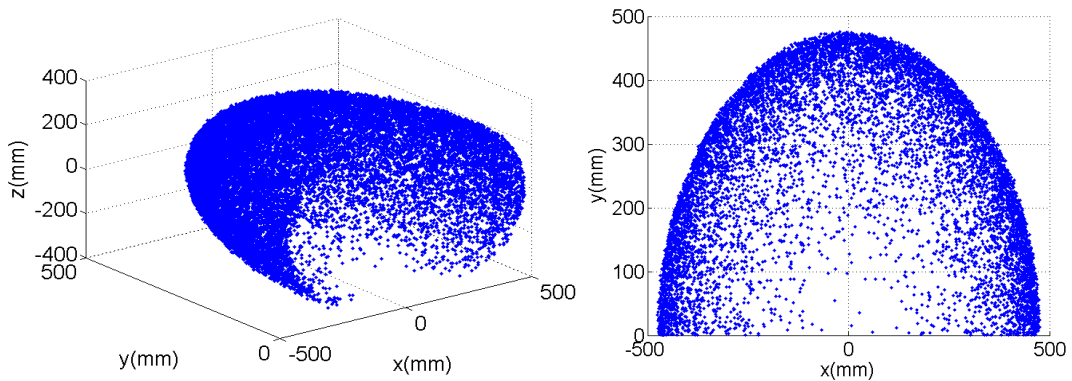


Fig. 14 Work space of elephant's trunk robot: (a) 3D view of work space, (b) Main section view of the work space

Cycled Equ. (14) for N times, and then obtain N random values of each unit. Substitute the obtained random values into the kinematics of the robot to obtain N random poses of the robot end in the base coordinate system.

The motion range between the units of the proposed elephant’s trunk robot is $[-90^\circ, -90^\circ]$, and the random point is 100000 points. The motion space of the elephant’s trunk robot is calculated as shown in Fig. 14.

6 EXPERIMENTS

An experimental prototype of the trunk robot was developed. The main parameters are shown in Table 2. The designed trunk robot includes a total of nine units including one base unit (unit 0) and eight actuation units (units 1–8). The end-unit of the eight actuation units (unit 8) is small in size and mainly serves as an assist. Thus, when data is collected, the focus is on seven actuation units (units 1–7). The link parameters of these units are shown in Table 4.

Table 4. Unit link lengths

Unit number	Value
Unit 1 BLL(bottom link length)	79.73mm
Unit 2 BLL	74.96mm
Unit 3 BLL	70.19mm
Unit 4 BLL	64.69mm
Unit 5 BLL	60.12mm
Unit 6 BLL	54.90mm
Unit 7 BLL	49.64mm
Unit 1 SLL(support link length)	84.91mm
Unit 2 SLL	80.45mm
Unit 3 SLL	74.79mm
Unit 4 SLL	69.45mm
Unit 5 SLL	64.89mm
Unit 6 SLL	60.60mm
Unit 7 SLL	54.92mm

When the elephant's trunk robot holds an object, the measurement of the change in the rotation angle of the robot during the holding process is performed by arranging a potentiometer at each revolute joint, as discussed above. The potentiometer accuracy is 1% and the measurement range is 50 kΩ. The initial angle when the angle of each joint is obtuse is predefined, so when the robot holds the object, the angle between each joint will continue to decrease.

Here we focus on representative experiments showing free bending and stretching experiments (Fig. 15) of the trunk robot, including grasping and holding a basketball and tubes. Figs. 16 and 17 depict curves showing the variation of the angles of the joints of the trunk robot during a typical grasping operation. As can be observed from the figures, the angles between the various joints are continually decreasing as the elephant's trunk robot moves closer to the target during each operation. This denotes the process of self-adaptive contact between the robot and the held object. Finally, the angles of all joints tend to assume a fixed value, which indicates that the trunk robot achieves a stable grip on the target. The test results verify that the robot achieves the desired functionality. Under the single-motor drive, it can realize the bending function and the adaptive holding function for objects with a range of different shapes and sizes. It should

be noted that owing to unavoidable machining and assembly errors, and rotational friction (roller bearings are not placed in the rotating pair), these factors interact with the spring inside the robot during the bending process. At the initial moment of the robot's bending and the final moment of holding, individual units will experience motion lags or local anomalies. More details on the experiments are presented below.

Free bending and extension experiment of the elephant's trunk robot

As shown in Fig. 15, the motor drives the scissors mechanism to drive unit 1 to rotate. The bending angles of the other units are different, and a final accurate hold shape is attained after 20 s.

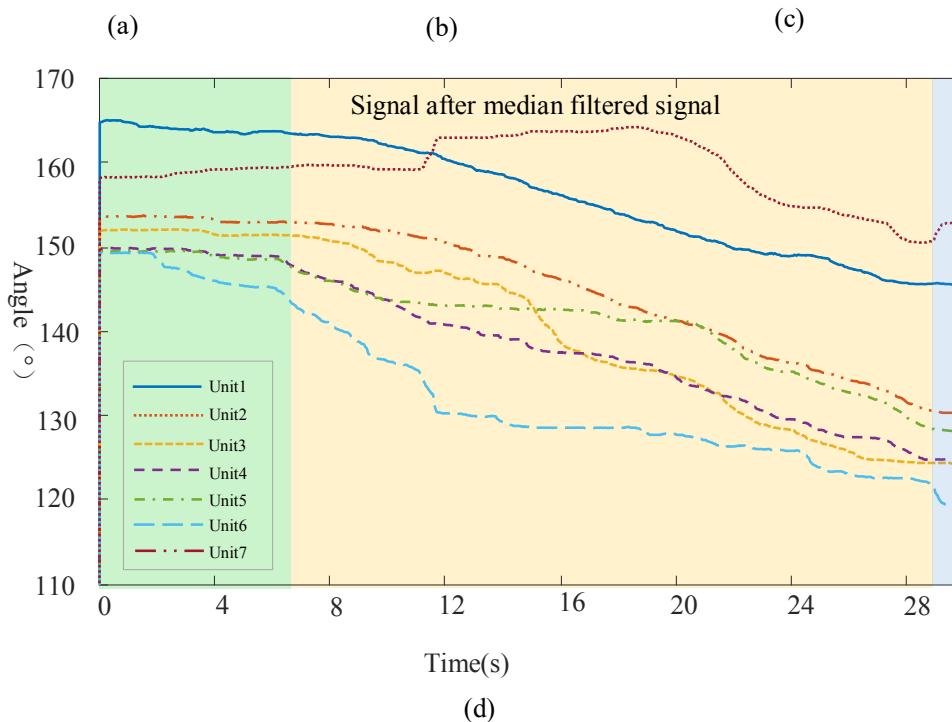
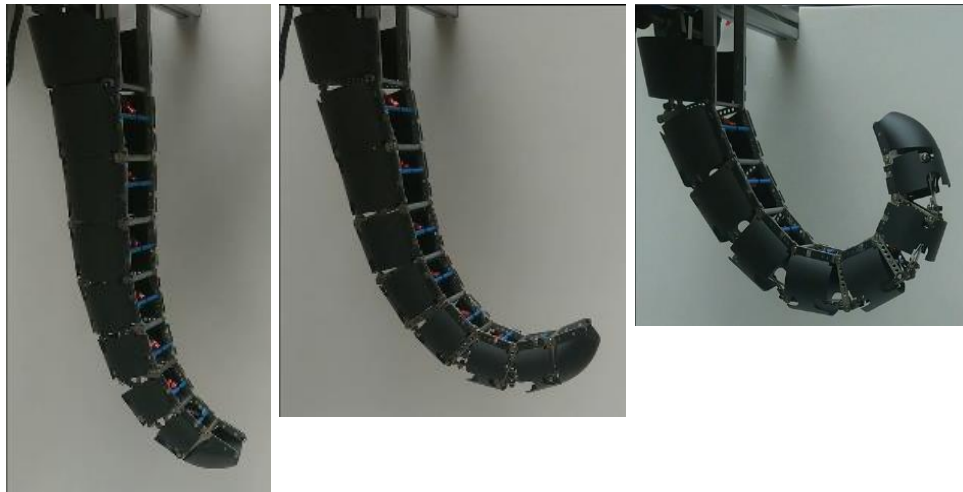


Fig. 15 Free bending experiments: (a) initial robot pose, (b) Intermediate bending process, (c) bending final pose, (d) curve of each unit rotation angle during bending

As shown in Fig. 15(d), at the initial time, the rotation angle of each unit is relatively small. After a certain period of time, the rotation speed of each unit suddenly increases, and the slope of the curve is increased. However, when an almost uniform rotation is maintained, the slope of the curve is unchanged. Furthermore, there is no crossover phenomenon in the corner curves of each unit. At the last moment, the slope of the corner curve suddenly becomes smaller and becomes nearly straight, as the robot bends to the final posture.

Elephant's trunk robot holds unfixed basketball

As shown in Fig. 16, the motor drives the scissors mechanism to drive unit 1 to rotate, and the bending angles of the other units are different. After 20s, the unfixed and free-standing ball is held firmly.

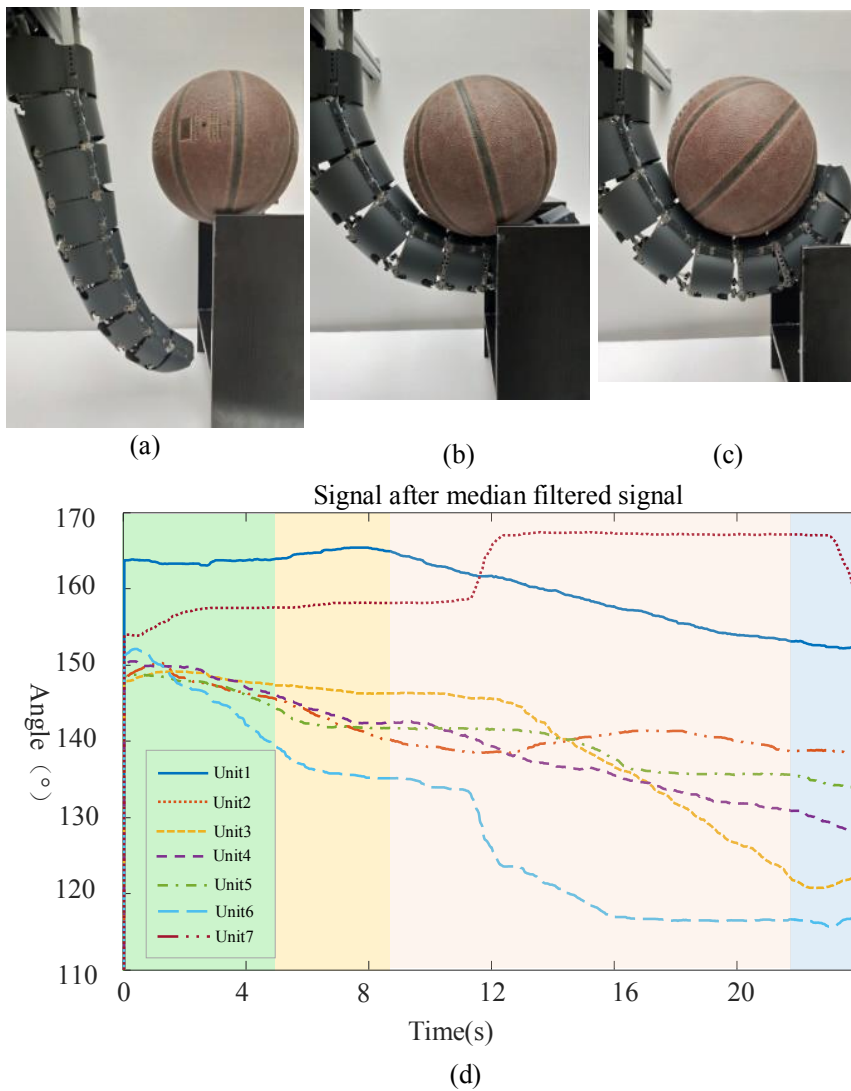


Fig. 16 Holding a non-fixed sphere experiment: (a) initial robot pose, (b) contact with sphere, (c) lifting sphere, and (d) angle curve: rotating each unit during holding

As shown in Fig. 16 (d), at the initial time, the rotation angle of each unit is relatively small. After a period of time, the rotation speed of each unit suddenly increases, and the slope of the curve is increased.

However, when the rotation speed is maintained at a nearly uniform speed, the slope of the curve is basically unchanged. In addition, there is no crossover phenomenon in each unit corner curve. When the robot is in contact with the sphere, the curvatures of the corners of all units change significantly, and a crossover phenomenon occurs. This is a process in which the robot automatically adapts to the shape of the sphere and holds it. At the last moment, the slope of the corner curve suddenly becomes smaller and nearly straight, and the robot bends to assume the final posture.

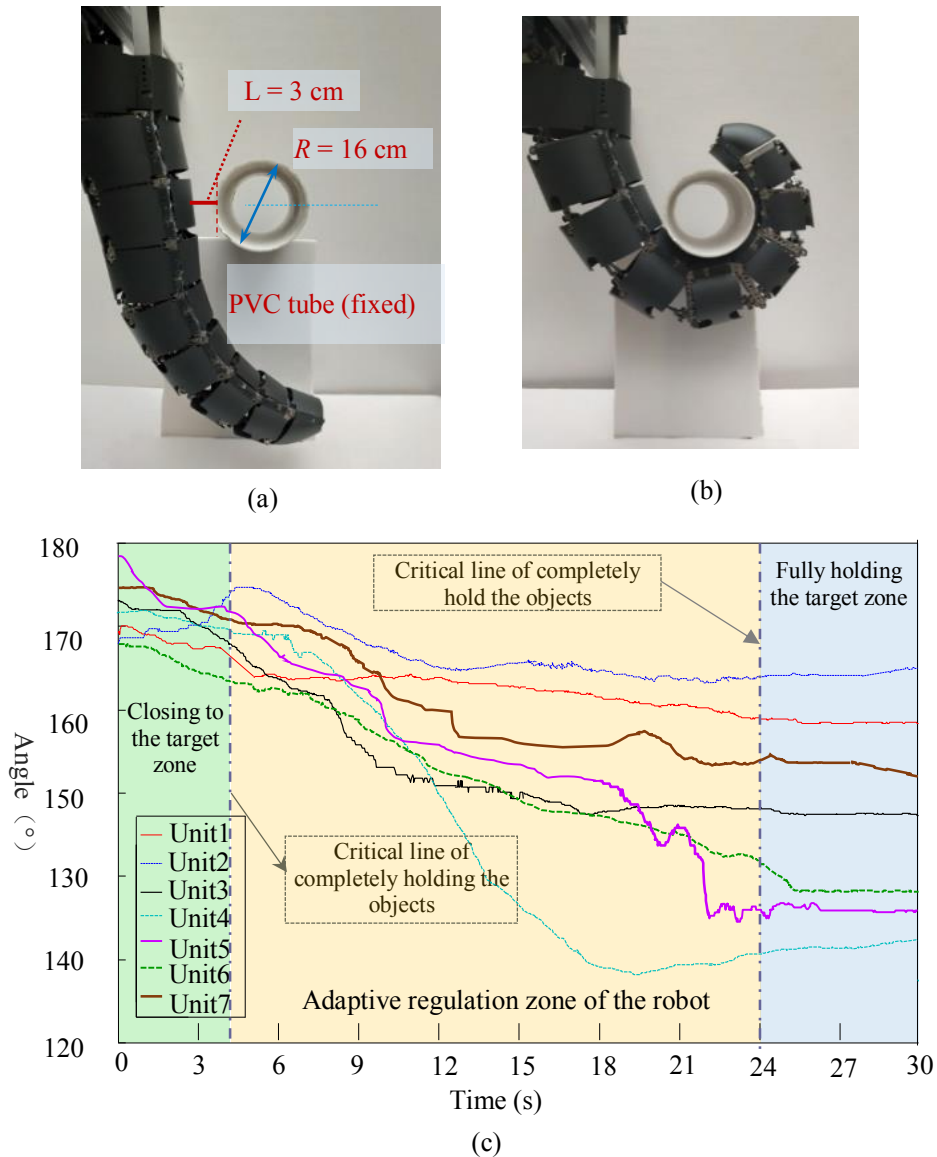


Fig. 17 Tubular holding experiments at fixed positions: (a) initial robot pose, (b) final posture after hold, and (c) curve of each unit rotation angle during hold

Self-adaptive tubular holding experiment for the elephant's trunk robot

As shown in Fig. 17, the robot holds a 16cm diameter tube at a fixed position. At the initial time, the tube is 3cm away from the third unit of the robot. When held, the motor drives the scissors mechanism to drive unit 1 to rotate, while the bending angles of the other units are different. After 20s, the stationary

tube is held in a stable manner. As shown in Fig. 17(c), at the initial time, the change curve of the rotation angle between each unit is reduced synchronously, and the robot moves closer to the target. After a period of time, the curvature of the rotation of each unit suddenly changes significantly. The value of the joint angle of the unit that first touches the target tends to be close to a constant value at subsequent time instants, while the end-unit continues to hold the target, and the curve of the angle change continues to decrease in the last time period. The curve of the angle variation of the unit does not change any further but is maintained at a fixed value, thereby indicating that the robot has completed the full grasping of the target object.

Soft shell prototype holding operation experiment

A “soft shell” cover for the robot was developed, in order to enhance the robustness of the grasps. The soft shell prototype in various experiments is shown in Fig. 18. From these experiments, we observe that the robot with soft shell has improved adaptability to adapt to the shape of the objects compared with the hard shell prototype.

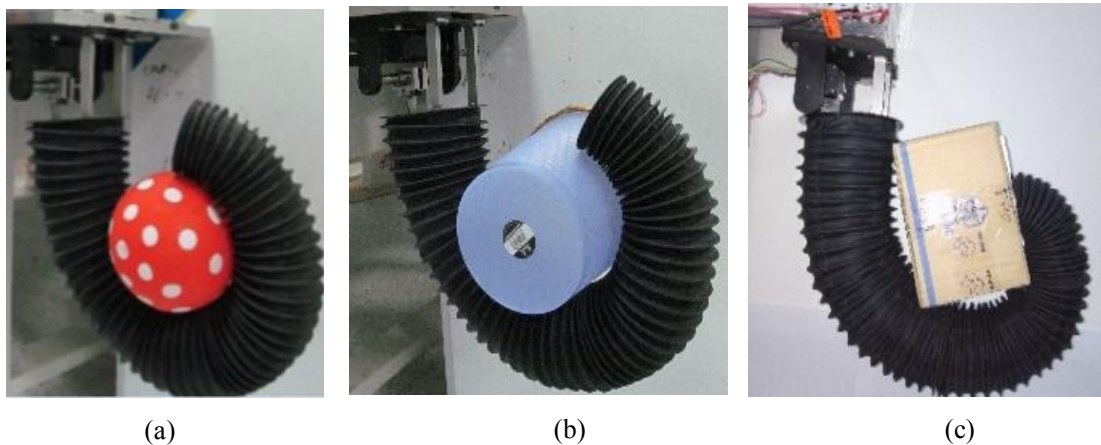


Fig. 18 Grasping experiment with soft shell cover: (a) trash can, (b) packing box, (c) elastic ball

Maximum adaptive load experiment

Load a different number of masses in the carton and convert them to gravity to simulate different loads. When the mass is 3 kg, the total load of the carton and the mass is calculated to be 30.7N. At this time, the spring compression amount of the penultimate section reaches the maximum value as shown in Fig. 19. Therefore, under the current holding state, the elephant’s trunk robot can withstand a maximum load of 30.7N while ensuring self-adaptation.

The spring stiffness of the prototype is 0.5 N/mm. If the spring stiffness increases, the maximum load that the structure withstands under its adaptive characteristics will increase.

When the holding load exceeds 30.7N, the holding function can also be realized, but the adaptive characteristics of the elephant’s trunk robot will disappear. The maximum load that can be carried afterwards is the load that destroys the structure of the elephant’s trunk robot.

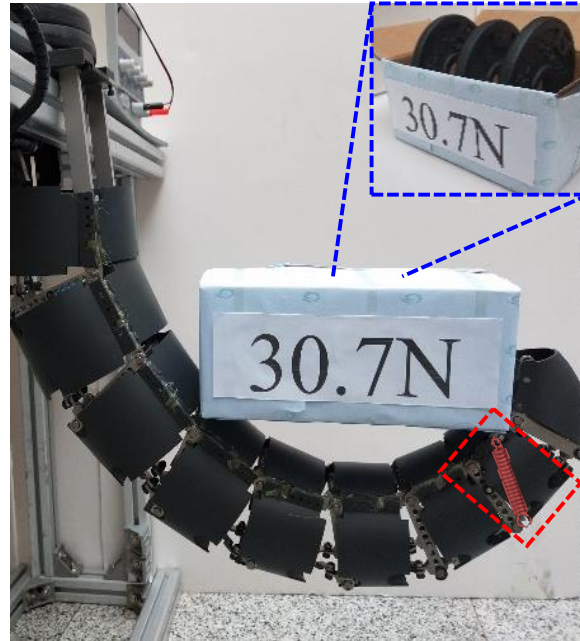


Fig. 19 Maximum adaptive load experiment

7 CONCLUSIONS

In this paper, we introduce the novel design and present supporting analysis and experimental testing of a new type of elephant trunk robot. This manipulator has redundant degrees-of-freedom and is under-actuated, with actuation provided by a single motor. The springs constraining the unactuated degrees-of-freedom contribute to the smooth and natural profile of the arm's motion. They also provide significant compliance in the structure, which allows conformance to environmental constraints upon contact, yielding the potential of adaptive whole arm manipulation. The main innovation involves a modification of the traditional form of robotic under-actuated mechanism using a scissors mechanism. This allows the manipulator to bend quickly and freely into a wide variety of postures, providing a significantly improved workspace in cluttered environments.

8 ACKNOWLEDGMENTS

The authors express their gratitude to the referees for very carefully reading and constructive comments and detailed suggestions which have improved this paper. This study is supported by National Key R&D Program of China (2018YFB1304600), National Natural Science Foundation of China (51605474, 61821005), and CAS Interdisciplinary Innovation Team (JCTD-2018-11).

REFERENCES

- [1] Trivedi, D., Rahn, C.D., Kier, W.M., and Walker, I.D., 2008, “Soft Robotics: Biological Inspiration, State of the Art, and Future Research”, *Appl. Bionics. Biomech.*, 5(2), pp. 99-117.
- [2] Axinte, D., Dong, X., Palmer, D., et al, 2018, “MiRoR—Miniaturized Robotic Systems for Holistic In-Situ Repair and Maintenance Works in Restrained and Hazardous Environments”, *IEEE-ASME T. Mech.*, 23(2), pp: 978-981.
- [3] Burgner-Kahrs, J., Rucker, D. C., and Choset, H., 2015, “Continuum Robots for Medical Applications: A Survey”, *IEEE T. Robot.*, 31(6), pp: 1261-1280.
- [4] Dong, X., Axinte, D., Palmer, D., et al, 2017, “Development of a slender continuum robotic system for on-wing inspection/repair of gas turbine engines,” *Robot. Cim-Int. Manuf.*, 44, pp. 218–229.
- [5] Webster, R. J. and Jones, B. A., 2010, “Design and Kinematic Modeling of Constant Curvature Continuum Robots: A Review”, *Int. J. Robot. Res.*, 29(13), pp. 1661-1683.
- [6] Hirose, S. and Yamada, H., 2009, “Snake-like Robots [Tutorial]”, *IEEE Robot. Autom. Mag.*, 16(1), pp. 88-98.
- [7] Walker, I. D., Choset, H., and Chirikjian, G., 2016, “Snake-like and Continuum Robots”, *Springer Handbooks of Robotics*. Siciliano, B., Khatib, O., eds., Springer, Cham, pp. 481-498.
- [8] Lipson, H., 2014, “Challenges and Opportunities for the Design, Simulation, and Fabrication of Soft Robots”, *Soft. Robot.*, 1(1), pp. 12-20.
- [9] Majidi, C., 2014, “Soft Robotics: A Perspective – Current Trends and Prospects for the Future”, *Soft. Robot.*, 1(1), pp. 2-11.
- [10] Gravagne, I., Rahn, C. D., and Walker I.D., 2003 “Large deflection dynamics and control for planar continuum robots”, *IEEE-ASME T. Mech.*, 8(2), pp: 299-307.
- [11] Gravagne, I. and Walker, I. D., 2002, “Manipulability, force, and compliance analysis for planar continuum manipulators”, *IEEE T. Robot. Autom.*, 18(3), pp: 263-273.
- [12] Buckingham, R., 2002, “Snake arm robots”, *Ind. Robot.*, 29(3), pp: 242-245.
- [13] Camarillo, D. B., Milne, C. F., Carlson, C. R., et al, 2008, “Mechanics modeling of tendon-driven continuum manipulators”, *IEEE T. Robot.*, 24(6), pp: 1262-1273.
- [14] Yip, M. C. and Camarillo, D. B., 2014, “Model-less feedback control of continuum manipulators in constrained environments”, *IEEE T. Robot.*, 30(4), pp: 880-889.
- [15] Hu, H., Wang, P., Sun, L., et al, 2010, “Kinematic Analysis and Simulation for Cable-driven Continuum Robot”, *Chin. J. Mech. Eng-En*, 46(19), pp: 1-8.
- [16] Ayvali, E. and Desai, J. P., 2012, “Towards a Discretely Actuated Steerable Cannula”, *ICRA.*, St. Paul, MN, pp. 1614-1619.
- [17] Rucker, D. C., Jones, B. B., and Webster, R.J., 2010, “A geometrically exact model for externally loaded concentric-tube continuum robots”, *IEEE T. Robot.*, 26(5), pp: 769-780.
- [18] Rone, W. S., and Ben-Tzvi, P., 2014, “Mechanics modeling of multisegment rod-driven continuum robots”, *J. Mech. Robot.*, 6(4), pp: 041006.
- [19] Dupont, P., Lock, J., and Butler, E., 2009, “Torsional Kinematic Model for Concentric Tube Robots”, *ICRA.*, Kobe, Japan, pp. 3851-3858.
- [20] Torres, L. G. and Alterovitz, R., 2011, “Motion Planning for Concentric Tube Robots Using Mechanics-based Models”, *IROS.*, San Francisco, CA, pp. 5153-5159.
- [21] Wei, W. and Simaan, N., 2012, “Modeling, Force Sensing, and Control of Flexible Cannulas for Microstent Delivery”, *J. Dyn. Syst-T. ASME*, 134(4), pp: 1-12.

- [22] Flint, P., Simaan, N., Taylor, R., 2004, "High Dexterity Snake-Like Robotic Slaves for minimally Invasive Telesurgery of the Upper Airway", MICCAI., Saint-Malo, France, pp. 17-24.
- [23] Jones, B. A. and Walker, I. D., 2006, "Kinematics for multisection continuum robots", IEEE T. Robot., 22(1), pp: 43-55.
- [24] Jones, B. A. and Walker, I. D., 2006, "Practical kinematics for real-time implementation of continuum robots", IEEE T. Robot., 22(6), pp: 1087-1099.
- [25] Mahl, T., Hildebrandt, A., and Sawodny, O., 2014, "A variable curvature continuum kinematics for kinematic control of the bionic handling assistant", IEEE T. Robot., 30(4), pp: 935-949.
- [26] Ranzani, T., Gerboni, G., Cianchetti, M., 2015, et al, "A bioinspired soft manipulator for minimally invasive surgery", Bioinspir. Biomim., 10(3), pp: 035008.
- [27] Godage, I. S., Nanayakkara, T., and Caldwell, D.G., 2012, "Locomotion with Continuum Limbs", IROS., Vilamoura, Portugal, pp. 293-298.
- [28] Marchese, A., Komorowski, K., Onal, C. D. and Rus, D., 2014, "Design and Control of a Soft and Continuously Deformable 2D Robotic Manipulation System", ICRA., Hong Kong, pp. 2189-2196.
- [29] Cieslak, R. and Morecki, A., 1999, "Elephant Trunk Type Elastic Manipulator – A Tool for Bulk and Liquid Type Materials Transportation," Robotica., 17, pp. 11-16.
- [30] Hannan, M. W. and Walker, I. D., 2003, "Kinematics and the Implementation of an elephant's trunk manipulator and other continuum style robots," J. Robotic. Syst., 20(2), pp. 45-63.
- [31] Tsukagoshi, H., Kitagawa, A. and Segawa, M., 2001, "Active Hose: An Artificial Elephant's Nose with Maneuverability for Rescue Operation," ICRA., Seoul, Korea, pp. 2454-2459.
- [32] Wilson, J. F., Li D., Chen, Z. and George, R. T., 1993, "Flexible Robot Manipulators and Grippers: Relatives of Elephant Trunks and Squid Tentacles", Robots and Biological Systems: Toward a New Bionics? Dario, P., Sandini, G., Aebischer, P., eds., Springer, Berlin, Heidelberg, pp. 474-479.
- [33] Bischof, B., Kirstein, L., Starke, J., et al, "ROGER- Robotic geostationary orbit restorer", 34th COSPAR Scientific Assembly, The Second World Space Congress, Houston, TX, USA, October 10-19, 2002, 109, pp: 183-193.
- [34] Huang, Z., Liu, J., Li, Q., 2008, "A Unified Methodology for Mobility Analysis Based on Screw Theory", Smart Devices and Machines for Advanced Manufacturing. Wang, L., Xi, J. eds., Springer, London, pp: 49-59.

Figure Captions List

Figure number and the page number	Captions
Figure 1 (Page. 4)	Elephant's trunk robot: (a) dimensions, (b) hard shell, and (c) soft shell
Figure 2 (Page. 6)	Driving principle: All units are driven by the same motor
Figure 3 (Page. 7)	Robot grasps objects of different shapes and sizes: (a) holding irregularly shaped objects, and (b) holding polygonal objects
Figure 4 (Page. 7)	Robot grasps objects at different positions: (a) holding a proximal target, and (b) holding a closer target
Figure 5 (Page. 8)	Robot used in space extreme environments: (a) holding a satellite body that rotates around an isometric axis and (b) holding a satellite solar windsurfer that rotates around a central axis (Size parameters can be designed according to the specific needs of the space application)
Figure 6 (Page. 9)	Mechanical design of the core robot units
Figure 7 (Page. 10)	Mechanical design of the base unit and unit 1
Figure 8 (Page. 11)	Schematics of the kinematic unit and motion pair–screw coordinate system: (a) two-unit schematic, (b) scissors mechanism, (c) left part of the scissors mechanism, and (d) right part of the scissors mechanism
Figure 9 (Page. 15)	Elephant's trunk robot flowchart
Figure 10 (Page. 16)	(a) Initial angle of unit k and unit $(K+1)$ with different positions of the spring, (b) trajectory of the robot with different positions of spring
Figure 11 (Page. 17)	F-k curve: (a) Relationship between the force and the stiffness coefficient of the spring, and (b) relationship between the angle and the change rate of the stiffness of the spring

Figure 12 (Page. 18)	Control system diagram of the robot:(a) system composition, and (b) control system model
Figure 13 (Page. 19)	DH coordinate system of elephant's trunk robot
Figure 14 (Page. 20)	Work space of elephant's trunk robot: (a) 3D view of work space, (b) Main section view of the work space
Figure 15 (Page. 22)	Free bending experiments: (a) initial robot pose, (b) Intermediate bending process, (c) bending final pose, (d) curve of each unit rotation angle during bending
Figure 16 (Page. 23)	Holding a non-fixed sphere experiment: (a) initial robot pose, (b) contact with sphere, (c) lifting sphere, (d) holding posture, and (e) angle curve: rotating each unit during holding
Figure 17 (Page. 24)	Tubular holding experiments at fixed positions: (a) initial robot pose, (b) final posture after hold, and (c) curve of each unit rotation angle during hold
Figure 18 (Page. 25)	Grasping experiment with soft shell cover: (a) trash can, (b) packing box, (c) elastic ball
Figure 19 (Page. 26)	Maximum adaptive load experiment

Table Caption List

Table number and the page number	Captions
Table 1 (Page. 3)	Comparison of different types of continuum robots
Table 2 (Page. 5)	Parameters of the robot
Table 3 (Page. 19)	Parameters of DH coordinate system of elephant's trunk robot
Table 4 (Page. 21)	Unit link lengths